The non-thermal emission following GW170817 is consistent with a conical radially-stratified outflow with initial Lorentz factor $\lesssim 10$

Gilad Sadeh[★], Eli Waxman
Dept. of Particle Phys. & Astrophys., Weizmann Institute of Science, Rehovot 76100, Israel

ABSTRACT

We show that the non-thermal radio to X-ray emission following the neutron star merger GW 170817 is consistent with synchrotron emission from a collisionless shock driven into the interstellar medium (ISM) by a conical radially stratified outflow observed ≈ 0.25 rad off-axis, with a power-low mass dependence on momentum, $M(> \gamma\beta) \propto (\gamma\beta)^{-5}$, maximum Lorenz factor $\gamma \approx 10$, opening (half-)angle ≈ 0.2 rad, and total energy of $\approx 10^{51}$ erg. The temporal dependence of the flux during its rising phase is determined by the radial stratification structure, which determines the rate at which outflow energy is deposited in the ISM. This is in contrast with highly relativistic, $\gamma \approx 100$, structured jet models, where the angular jet structure determines the time dependence through the gradual "unveiling" by deceleration of larger angular sections of the jet (which are initially "hidden" by relativistic beaming), typically leading to a predicted flux decline after the peak that is faster than observed. Our model predicts a dependence on the observing angle, which is different than that predicted by highly relativistic jet models. Particularly, similar merger events observed closer to the symmetry axis are predicted to show a similarly extended duration of flux increase with time. Our analysis demonstrates that the data do not require a highly relativistic $\gamma \approx 100$ component, but the presence of such a component with opening angle $\ll 0.2$ rad and energy $\ll 10^{51}$ erg cannot be excluded.

Key words: (transients:) neutron star mergers – (transients:) black hole-neutron star mergers – gravitational waves – radio continuum: transients – relativistic processes

1 INTRODUCTION

GW170817 provided the first opportunity for a detailed investigation of the off-axis synchrotron emission driven by a collimated relativistic outflow, with a long duration rich set of observations of the non-thermal radio, optical and X-ray emission (Hallinan et al. 2017; Troja et al. 2017; Lyman et al. 2018; Troja et al. 2020; Makhathini et al. 2021) and a measurement of emission centroid motion (Mooley et al. 2018a; Ghirlanda et al. 2019; Mooley et al. 2022).

• The observed spectrum is time independent and follows the expected synchrotron spectrum, $F_\nu \propto \nu^{(1-p)/2}$ (where p is the relativistic electrons' spectral index, $dn_e/d\gamma_e \propto \gamma_e^{-p}$), with $p = 2.17$ (Margutti et al. 2018; Troja et al. 2020; Makhathini et al. 2021), and with no indication for spectral breaks, implying that the synchrotron cooling, self-absorption and peak frequencies are outside the observed frequency range at all observed times.

• The light curve shows an initial achromatic rising phase, $F_\nu \propto t^{0.9}$ until ≈ 150 days (Alexander et al. 2018; Dobie et al. 2018; D'Avanzo et al. 2018), followed by a steep decline of $F_\nu \propto t^{-1.9}$ up to ~ 1000 days (Makhathini et al. 2021; Balasubramanian et al. 2022; Troja et al. 2022).

• The radio center of light position was measured by the VLBI at 75, 207, and 230 days after the merger (Mooley et al. 2018a;

Ghirlanda et al. 2019), complemented by an astrometric measurement of the optical kilonova location eight days after the merger. These measurements indicate a superluminal motion of the center of light implying a $\gamma \gtrsim 5$ outflow (Mooley et al. 2018a, 2022).

The moderate $F_\nu \propto t^{0.9}$ flux rise is inconsistent with that predicted for an ultra-relativistic jet with a uniform distribution of energy per solid angle ("top-hat") observed off-axis (Margutti et al. 2018; Mooley et al. 2018b; Gill et al. 2019). Furthermore, the gamma-ray emission associated with GW170817, GRB 170817A, is also inconsistent with such an interpretation (Kasliwal et al. 2017; Granot et al. 2017; Matsumoto et al. 2019). Thus, jets with various angular structures were considered in an attempt to explain the observations (Troja et al. 2019; Fong et al. 2019; Lamb et al. 2019; Hajela et al. 2019; Wu & MacFadyen 2019; Ryan et al. 2020; Takahashi & Ioka 2020).

In the highly relativistic "structured jet" models, the jet properties (e.g. energy per unit solid angle) vary as a function of the angle with respect to the jet axis. Most papers fitting structured jet models to the obsrved non-thermal light curve of GW170817 use semi-analytic codes, such as "afterglowpy", for the emission predicted for given model parameters, combined with an MCMC parameter estimation pipeline (Hajela et al. 2019; Lamb et al. 2019; Ghirlanda et al. 2019; Wu & MacFadyen 2019; Troja et al. 2019; Ryan et al. 2020; Troja et al. 2020; Makhathini et al. 2021; Ryan et al. 2023; McDowell & MacFadyen 2023; Palmese et al. 2024; Pellouin & Daigne 2024; Morsony et al. 2024; Wang et al. 2024; Nedora et al. 2024). These models typically cannot account

simultaneously for both the light curve and the centroid motion, and they typically do not include an accurate treatment of the jet sideways expansion, which considerably modifies the predictions for the light curve decline phase. Furthermore, the jet energy inferred in some of these models is typically $\sim 10^{52}$ erg, a relatively high value that corresponds to an isotropic equivalent energy $> 10^{54}$ erg, which is inconsistent with short GRB observations (D'Avanzo et al. 2014).

A more numeric approach to fitting structured jet models to the data was adopted in several papers, based on using numeric 2D hydrodynamic calculations (Mooley et al. 2018a; Gill et al. 2019; Gottlieb et al. 2019), approximate 1D hydrodynamic calculations (Mooley et al. 2022), and numerically calibrated (to ultra-relativistic structured jet calculations) analytic models (Govreen-Segal & Nakar 2023). These analyses typically find a jet opening angle of $\theta_j \sim 3° - 6°$ and a viewing angle of $\theta_v \sim 15° - 30°$ with respect to the jet axis. The decline of the flux after its peak time is typically predicted in these models to be faster than observed up to ~ 1000 days. This is due to the fact that the phase of increasing observed flux extends up to the time when deceleration unveils the full angular extent of the jet to the observer, and is then followed by a rapid flux decline that gradually shallows to an asymptotic $F_\nu \propto t^{-p}$ behavior, while the observed decline is shallower than t^{-p} (with $p = 2.17$).

In this paper, we show that the non-thermal emission is consistent with synchrotron emission from a collisionless shock driven into the ISM by a conical radially stratified outflow observed off-axis, with a power-low mass dependence on momentum, $M(> \gamma\beta) \propto (\gamma\beta)^{-5}$ and $\gamma \lesssim 10$. In this model, the peak in observed flux is obtained when the reverse shock, which is driven into the ejecta and decelerates it due to the interaction with the ISM, crosses through the ejecta (for highly relativistic, $\gamma \approx 100$, outflow the reverse shock crosses the ejecta and all the energy is transferred to the ISM at smaller radii, $r \propto \gamma^{-2/3}$, corresponding to much earlier observed times preceding the first radio detection). A shallow decline past peak is obtained for radially stratified outflows in cases where the reverse shock crosses through the ejecta before the deceleration reveals the full outflow extent to an off-axis observer.

The paper is organized as follows. In § 2, we present a simple semi-analytic method to calculate the synchrotron emission from a conical stratified outflow. 2D numeric calculations are presented in § 3. The accuracy of our semi-analytic calculations is determined in § 4 through a comparison to the numeric results. In all calculations, we assume that electrons are accelerated by the collisionless shock to power-law energy distribution, $dn_e/d\gamma_e \propto \gamma_e^{-p}$ where γ_e is the electron Lorenz factor (in the plasma rest frame), and that fractions ε_e and ε_B of the post-shock thermal energy are carried by non-thermal electrons and magnetic fields, respectively. In § 5 we show, using both semi-analytic and numeric calculations, that the stratified outflow model may account for the non-thermal emission following GW170817. Our conclusions are summarized in § 6.

2 A SEMI-ANALYTIC DERIVATION OF THE FLUX PRODUCED BY A CONICAL STRATIFIED OUTFLOW

2.1 Initial ejecta structure

We consider a radially stratified double-sided conical ejecta with opening angle θ_{open} (see Fig. 1), an angle-independent structure, and an initial power-law dependence of mass on momentum,

$$M(> \gamma\beta) = M_c \left(\frac{\gamma\beta}{\gamma_c\beta_c} \right)^{-k} \text{ for } \gamma_c\beta_c < \gamma\beta. \tag{1}$$
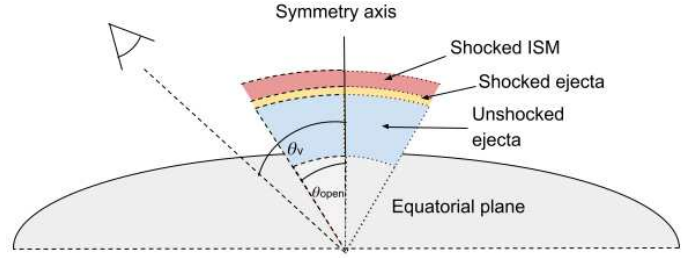

Figure 1. A schematic illustration showing a 2D slice of the 3D conical ejecta (described in § 2.1), and the forward-reverse shock structure that is formed and described in § 2.3. The symmetry axis corresponds to the azimuthal symmetry of the cone. θ_{open} is the initial cone opening angle. θ_v is the angle between the symmetry axis and the line of sight, such that $\theta_v = \pi/2$ corresponds to the equatorial plane.

2.2 Coordinate systems

The natural coordinate system for describing the ejecta and its hydrodynamic evolution is a spherical coordinate system (R, ϕ, θ), where R is the distance from the origin, ϕ is the azimuthal angle, and θ is the polar angle measured with respect to the ejecta symmetry axis (see Fig. 1).

To calculate the synchrotron emission, it is convenient to define a coordinate system with a pole aligned with the line of sight, which makes an angle θ_v with the ejecta symmetry axis. We therefore define another spherical coordinate system, (R, φ, ξ), where φ is the azimuthal angle (chosen such that $\varphi = 0$ corresponds to the equatorial plane in the case of $\theta_v = \pi/2$), ξ is the polar angle, and the pole is aligned with the line of sight. The coordinate transformation is

$$\cos\xi = \cos\theta_v \cos\theta - \sin\theta_v \sin\theta \sin\phi,$$
$$\sin\varphi = \frac{\cos\theta - \cos\theta_v \cos\xi}{\sin\xi \sin\theta_v}. \tag{2}$$

A cylindrical coordinate system, (r, φ, z), such that the z-axis is aligned with the line of sight, is useful for the semi-analytic calculation presented below. For this coordinate system, the coordinate transformation is

$$R = \sqrt{r^2 + z^2},$$
$$\tan\theta = \frac{\sqrt{(r\cos\varphi)^2 + (r\sin\varphi \cos\theta_v - z\sin\theta_v)^2}}{r\sin\varphi \sin\theta_v + z\cos\theta_v}. \tag{3}$$

2.3 Semi-analytic calculation

As the ejecta expands, a forward shock is driven into the ISM, and a reverse shock is driven into the ejecta. In previous papers (Sadeh et al. 2023; Sadeh 2024a), we developed a semi-analytic calculation method for modeling the dynamics for the case of a stratified spherical ejecta with a velocity profile given by Eq. (1) propagating into a cold and uniform ISM. We have shown that this method provides an accurate approximation for the results of numeric 1D relativistic hydrodynamics calculations (Sadeh et al. 2023). Here, we slightly modify the values of numerically calibrated model parameters to obtain higher accuracy for the higher Lorentz factors considered in this paper.

We approximate the shocked plasma as two uniform layers between the shocks, separated by a contact discontinuity. In Sadeh (2024a), we showed that the sideways expansion does not affect the predicted emission significantly up to the time at which the reverse shock crosses the ejecta. This is due to the fact that at any given time, most of

the internal energy is deposited into the ISM by the newly decelerated shell of the ejecta, which has not yet undergone significant sideways expansion.

The time at which the reverse shock crosses the ejecta is given, for on-axis observers, by (Sadeh et al. 2023)

$$t_{\text{peak}} = 550 g(\beta_c) \left(\frac{M_{c,-4}}{n_{-2}} \right)^{\frac{1}{3}} \text{days}, \quad g(\beta_c) = \frac{1.5 - \sqrt{0.25 + 2\beta_c^2}}{\gamma_c^{\frac{1}{3}} \beta_c},$$

(4)

where $n = 10^{-2} n_{-2} \text{cm}^{-3}$ and $M_c = 10^{-4} M_{c,-4} M_\odot$. t_{peak} is the time at which the flux reaches its peak for an on-axis observer. For an off-axis observer with $\theta_{\text{v}} > \theta_{\text{open}}$, the peak time is delayed with respect to t_{peak} given by Eq. (4) due to the subsequent unveiling of angular sections hidden by relativistic beaming.

Prior to reverse shock crossing, the ejecta structure is well approximated by a conical section of a spherical expanding ejecta. The emissivity is thus approximated as

$$j'_\nu = \begin{cases} j'_\nu(e, \rho, \gamma) & \text{for} \quad 0 < \theta < \theta_{\text{open}}, \\ j'_\nu(e, \rho, \gamma) & \text{for} \quad \pi - \theta_{\text{open}} < \theta < \pi, \\ 0 & \text{otherwise}, \end{cases}$$

(5)

where e, ρ and γ are the radially dependent plasma proper energy density, proper density, and Lorenz factor, respectively, and the prime ($'$) denotes a quantity measured in the plasma frame.

The emissivity, observed intensity (I_ν), and flux (F_ν) are computed following the methodology outlined in Sadeh et al. (2024) for frequencies above the self-absorption/peak frequency and below the cooling frequency. Correspondingly, the center of light is calculated by

$$R_{\text{CoL}} = \frac{\frac{1}{D^2} \int \int r^2 \sin \varphi I_\nu \, dr \, d\varphi}{F_\nu}.$$

(6)

The coordinates on the sky are chosen such that the symmetry axis is at $\varphi = \pi/2$ (a reflection symmetry axis at $\varphi = \pi/2$), omitting the necessity to consider the $r \cos \varphi$ component.

3 2D NUMERICAL CALCULATION

3.1 Hydrodynamics

We use the RELDAFNA code (Klein 2023) to solve the 2D relativistic hydrodynamics equations. RELDAFNA is an Eulerian code employing the Godunov scheme, incorporating adaptive mesh refinement (AMR) and second-order accuracy in time and space integration. Its efficient parallelization enables high-resolution calculations, even for complex multiscale problems. RELDAFNA's accuracy was confirmed by comparing it with similar codes (Zhang & MacFadyen 2006; Meliani et al. 2007) using standard test problems.

In our calculations, we use an equation of state of an ideal fluid with a smoothly varying adiabatic index (between 5/3 to 4/3),

$$\hat{\gamma} = \frac{4 + \left(1 + 1.1 \frac{e}{\rho' c^2} \right)^{-1}}{3},$$

(7)

which is in very good agreement with the equation of state of a mildly relativistic fluid provided by Synge (1957). The 1.1 factor is introduced for better agreement with the exact solution in the range of $4 < e/\rho' c^2 < 9$ (corresponding to $5 < \gamma < 10$, Sadeh 2024a).

Our simulations were performed in a 2D cylindrical coordinate system (r, z) assuming axial symmetry, and applying reflective boundary conditions at both the symmetry axis ($r = 0$) and the symmetry plane ($z = 0$). The computational domain boundaries were set at $r = 10^{19}$ cm and $z = 10^{19}$ cm. The initial grid prioritizes resolving the ejecta by placing a higher concentration of cells within it, with a coarser spacing outside. Typically, the simulation begins with 500×500 cells, with most cells within the ejecta. AMR dynamically adjusts the resolution throughout the simulation, optimizing cell distribution along both the r and z axes to effectively capture regions of significant variation in pressure, density, or Lorentz factor. We systematically refined the initial spatial grid and temporal steps to assess convergence. We also iteratively increased the number of times the regridding scheme is allowed to multiply the number of cells within a time step. This process was continued until no significant changes were observed in the hydrodynamics and emergent flux.

The initial ejecta structure was chosen as described in § 2.1. The initial radius of a mass shell $M(> \gamma\beta)$ was determined as $r_0 = \beta c t_0$, with $t_0 \approx 10^6$ s. Behind the ejecta, between $r = \beta_c c t_0$ and $r = 0.99\beta_c c t_0$, we chose a smooth power-law interpolation between β_c, ρ_c (the density of slowest part the ejecta) and $\beta = 0$, $\rho = 10^{-3} \rho_{\text{ISM}}$ to avoid numeric instabilities due to discontinuities in the density and velocity. The initial pressure in all of the cells is set to $P = 10^{-10} \rho_{\text{ISM}} c^2$ where ρ_{ISM} is the ISM mass density.

3.2 Radiation

The observed flux was calculated following the same procedure described in detail in Sadeh (2024a).

For each cell in the 3D grid constructed for the calculation of radiation emission, we calculate the projected center of light along the symmetry axis of the 2D sky plane, $R \sin \xi \sin \varphi$, where φ is the azimuthal angle on the sky, see Eq. (2). The center of light is computed by averaging the different projections of each cell weighted by the flux contribution from it (ΔF_ν),

$$R_{\text{CoL}} = \frac{\Sigma_i^{\#\text{cells}} [R \sin \xi \sin \varphi]_i [\Delta F_\nu]_i}{F_\nu}.$$

(8)

4 SEMI ANALYTIC VS. NUMERICAL RESULTS

In Fig. 2, we compare the light curve (at frequencies above the self-absorption and peak frequency and below the cooling frequency) and the time-dependent light centroid location obtained semi-analytically with the results of the 2D numerical calculation. Recall that the semi-analytic description is valid up to time at which the reverse shock crosses the ejecta. The agreement is within 10's of percent for relevant values of $\{k, \gamma_c, n, M_c, \varepsilon_e, \varepsilon_B, p, \theta_{\text{open}}\}$.

5 GW170817

In Sadeh (2024b), we show that the absence of breaks from the non-thermal power-law spectrum of GW170817 implies that (i) the Lorentz factor of the plasma emitting the observed radiation is $\gamma > 2.6$ at $t \sim 10$ days and $\gamma < 12$ at $t > 16$ days, and (ii) $n \cdot \varepsilon_B \lesssim 3 \times 10^{-7} \text{cm}^{-3}$. Considering these constraints, we used our semi-analytic method to find parameter values that yield model predictions that are in reasonable agreement with observations. We then used the 2D numeric code to calculate more accurately the model predictions, and to extend them to times past the validity time of the semi-analytic approximation. We do not attempt to obtain a "best-fit" set of parameter values, as the real outflow structure is likely more complicated than the simplified structure that we are using for our model
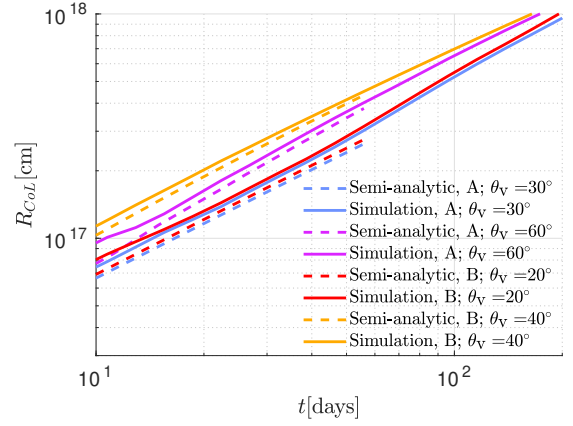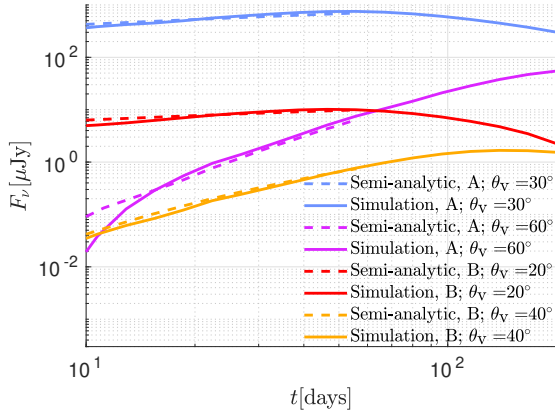
Figure 2. A comparison between the time-dependent flux (left panel) and the time-dependent light centroid location (right panel) obtained semi-analytically (solid lines) and numerically (dashed lines), for various viewing angles and two sets of parameter values $\{k, \gamma_c, n, M_c, \varepsilon_e, \varepsilon_B, p, \theta_{open}\}$ = A: $\{5, 3, 10^{-2}cm^{-3}, 10^{-1}M_\odot, 10^{-1}, 10^{-2}, 2.2, 30°\}$, B: $\{5, 3, 10^{-3}cm^{-3}, 10^{-2}M_\odot, 10^{-1}, 10^{-2}, 2.2, 20°\}$. The flux is shown for a distance of 100Mpc and a frequency of 6 GHz.
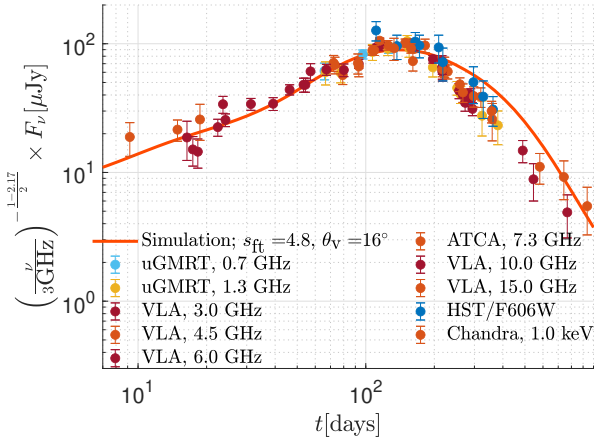
Figure 3. The non-thermal radio to X-ray flux (circles, Makhathini et al. 2021) of the electromagnetic counterpart of GW170817, compared to the results of a 2D numeric calculation of the emission driven by a stratified conical ejecta with $\{k, \gamma_c, n, M_c, \varepsilon_e, \varepsilon_B, p, \theta_{open}, \theta_v\}$ = $\{4.8, 6, 5 \times 10^{-4}cm^{-3}, 9 \times 10^{-3}M_\odot, 0.1, 2 \times 10^{-5}, 2.17, 10°, 16°\}$. The model ejecta is truncated beyond $\gamma = 12$.

Figure 4. The measured motion of the light centroid (circles, Mooley et al. 2018b, 2022) compared to the results of a 2D numeric calculation of the emission driven by a stratified conical ejecta with $\{k, \gamma_c, n, M_c, \varepsilon_e, \varepsilon_B, p, \theta_{open}, \theta_v\}$ = $\{4.8, 6, 5 \times 10^{-4}cm^{-3}, 9 \times 10^{-3}M_\odot, 0.1, 2 \times 10^{-5}, 2.17, 10°, 16°\}$. The model ejecta is truncated beyond $\gamma = 12$.

calculations, which also includes simplifying assumptions regarding the microphysics of particle acceleration and emission of radiation (e.g. fixed electron and magnetic field energy fractions, independent of shock parameters) We found that the following choice of parameters yields a good fit to the data: $\{k, \gamma_c, n, M_c, \varepsilon_e, \varepsilon_B, p, \theta_{open}, \theta_v\}$ = $\{4.8, 6, 5 \times 10^{-4}cm^{-3}, 9 \times 10^{-3}M_\odot, 0.1, 2 \times 10^{-5}, 2.17, 10°, 16°\}$ (Makhathini et al. 2021; Mooley et al. 2018b, 2022), as shown in Figs. 3-4. In the numeric calculation, the ejecta is truncated beyond $\gamma = 12$.

6 CONCLUSIONS

We have shown that the non-thermal radio to X-ray emission following the neutron star merger GW170817 is consistent with synchrotron emission from a collisionless shock driven into the interstellar medium (ISM) by a conical radially stratified outflow observed
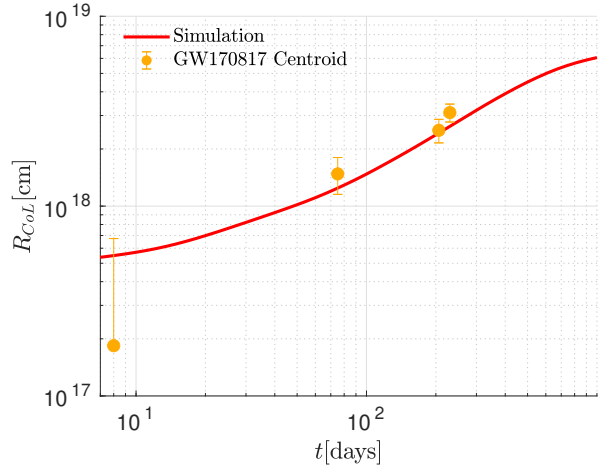
≈ 0.25 rad off-axis, with a power-low mass dependence on momentum, $M(> \gamma\beta) \propto (\gamma\beta)^{-5}$ over the range $5 \lesssim \gamma \lesssim 10$, opening (half-)angle ≈ 0.2 rad, and total energy of $\approx 10^{51}$erg. A comparison of the measured and model-predicted fluxes and light centroid motion is given in figures 3 and 4, for a specific choice of values of model parameters. We did not attempt to obtain a "best-fit" set of parameter values, as the real outflow structure is likely more complicated than the simplified structure that we are using for our model calculations, which also includes simplifying assumptions regarding the microphysics of particle acceleration and emission of radiation (e.g. fixed electron and magnetic field energy fractions, independent of shock parameters). The results of the 2D numeric calculations of the light curve and centroid motion agree with those of our semi-analytic approximation (valid up to the flux peak time, see figure 2), supporting the validity of both.

The temporal dependence of the flux during its rising phase is

determined in the radially stratified outflow model by the radial stratification structure, which determines the rate at which outflow energy is deposited in the ISM. This is in contrast with highly relativistic, $\gamma \approx 100$, structured jet models, where the angular jet structure determines the time dependence through the gradual "unveiling" by deceleration of larger angular sections of the jet (which are initially "hidden" by relativistic beaming). In the relativistic jet models, the viewing angle θ_v is required to be significantly larger than the opening angle θ_{open}, $\theta_v > 2\theta_{open}$ to allow for the observed rising flux phase, and the peak flux is obtained when the deceleration reveals the full angular extent of the jet to the observer, leading to a predicted flux decline after peak that is faster than observed. In the stratified outflow model, the rising flux does not require a large viewing angle, and the post-peak decline is consistent with the observed one.

The radially stratified outflow model predicts a dependence on the observing angle, which is different than that predicted by highly relativistic jet models. Particularly, similar merger events observed at smaller viewing angles are predicted in our model to show a similarly extended duration of flux increase with time. Our analysis demonstrates that the data do not require a highly relativistic $\gamma \approx 100$ component, but the presence of such a component with opening angle $\ll 0.2$ rad and energy $\ll 10^{51}$ erg cannot be excluded, and it may dominate the observed flux when observed on-axis. The rapid deceleration of such a component, compared to the deceleration of the slower $\gamma < 10$ outflow, will lead to a light curve that can be discriminated from that of the slower outflow.

Finally, we note that since flow structures that differ widely ($\gamma \sim 100$ relativistic jet and $\gamma < 10$ radially stratified outflow) may predict similar non-thermal flux when observed off-axis, one cannot accurately infer parameters, e.g. the viewing and opening angles, based on fitting models to the data. This also implies that an accurate determination of H_0 (Hotokezaka et al. 2019; Govreen-Segal & Nakar 2023; Palmese et al. 2024) is impossible through such parameter inference.

REFERENCES

Alexander, K. D., Margutti, R., Blanchard, P. K., et al. 2018, The Astrophysical Journal, 863, L18, doi: 10.3847/2041-8213/aad637

Balasubramanian, A., Corsi, A., Mooley, K. P., et al. 2022, The Astrophysical Journal, 938, 12, doi: 10.3847/1538-4357/ac9133

D'Avanzo, P., Salvaterra, R., Bernardini, M. G., et al. 2014, Monthly Notices of the Royal Astronomical Society, 442, 2342, doi: 10.1093/mnras/stu994

Dobie, D., Kaplan, D. L., Murphy, T., et al. 2018, The Astrophysical Journal, 858, L15, doi: 10.3847/2041-8213/aac105

D'Avanzo, P., Campana, S., Salafia, O. S., et al. 2018, Astronomy & Astrophysics, 613, L1, doi: 10.1051/0004-6361/201832664

Fong, W., Blanchard, P. K., Alexander, K. D., et al. 2019, The Astrophysical Journal, 883, L1, doi: 10.3847/2041-8213/ab3d9e

Ghirlanda, G., Salafia, O. S., Paragi, Z., et al. 2019, Science, 363, 968, doi: 10.1126/science.aau8815

Gill, R., Granot, J., Colle, F. D., & Urrutia, G. 2019, The Astrophysical Journal, 883, 15, doi: 10.3847/1538-4357/ab3577

Gottlieb, O., Nakar, E., & Piran, T. 2019, Monthly Notices of the Royal Astronomical Society, 488, 2405, doi: 10.1093/mnras/stz1906

Govreen-Segal, T., & Nakar, E. 2023, Monthly Notices of the Royal Astronomical Society, 524, 403, doi: 10.1093/mnras/stad1628

Granot, J., Guetta, D., & Gill, R. 2017, The Astrophysical Journal, 850, L24, doi: 10.3847/2041-8213/aa991d

Hajela, A., Margutti, R., Alexander, K. D., et al. 2019, The Astrophysical Journal, 886, L17, doi: 10.3847/2041-8213/ab5226

Hallinan, G., Corsi, A., Mooley, K. P., et al. 2017, Science, 358, 1579, doi: 10.1126/science.aap9855

Hotokezaka, K., Nakar, E., Gottlieb, O., et al. 2019, Nature Astronomy, 3, 940, doi: 10.1038/s41550-019-0820-1

Kasliwal, M. M., Nakar, E., Singer, L. P., et al. 2017, Science, 358, 1559, doi: 10.1126/science.aap9455

Klein, Y. Y. 2023, Construction of a Multidimensional Parallel Adaptive Mesh Refinement Special Relativistic Hydrodynamics Code for Astrophysical Applications, doi: 10.48550/arXiv.2310.02331

Lamb, G. P., Lyman, J. D., Levan, A. J., et al. 2019, The Astrophysical Journal, 870, L15, doi: 10.3847/2041-8213/aaf96b

Lyman, J. D., Lamb, G. P., Levan, A. J., et al. 2018, Nature Astronomy, 2, 751, doi: 10.1038/s41550-018-0511-3

Makhathini, S., Mooley, K. P., Brightman, M., et al. 2021, The Astrophysical Journal, 922, 154, doi: 10.3847/1538-4357/ac1ffc

Margutti, R., Alexander, K. D., Xie, X., et al. 2018, The Astrophysical Journal, 856, L18, doi: 10.3847/2041-8213/aab2ad

Matsumoto, T., Nakar, E., & Piran, T. 2019, Monthly Notices of the Royal Astronomical Society, 486, 1563, doi: 10.1093/mnras/stz923

McDowell, A., & MacFadyen, A. 2023, The Astrophysical Journal, 945, 135, doi: 10.3847/1538-4357/acbd8e

Meliani, Z., Keppens, R., Casse, F., & Giannios, D. 2007, Monthly Notices of the Royal Astronomical Society, 376, 1189, doi: 10.1111/j.1365-2966.2007.11500.x

Mooley, K. P., Anderson, J., & Lu, W. 2022, Nature, 610, 273, doi: 10.1038/s41586-022-05145-7

Mooley, K. P., Deller, A. T., Gottlieb, O., et al. 2018a, Nature, 561, 355, doi: 10.1038/s41586-018-0486-3

Mooley, K. P., Nakar, E., Hotokezaka, K., et al. 2018b, Nature, 554, 207, doi: 10.1038/nature25452

Morsony, B. J., De Los Santos, R., Hernandez, R., et al. 2024, Monthly Notices of the Royal Astronomical Society, 533, 510, doi: 10.1093/mnras/stae1638

Nedora, V., Crosato Menegazzi, L., Peretti, E., Dietrich, T., & Shibata, M. 2024, Multi-physics framework for fast modeling of gamma-ray burst afterglows, doi: 10.48550/arXiv.2409.16852

Palmese, A., Kaur, R., Hajela, A., et al. 2024, Physical Review D, 109, 063508, doi: 10.1103/PhysRevD.109.063508

Pellouin, C., & Daigne, F. 2024, The Very High Energy Afterglow of Structured Jets: GW 170817 and Prospects for Future Detections. https://ui.adsabs.harvard.edu/abs/2024arXiv240608254P

Ryan, G., van Eerten, H., Piro, L., & Troja, E. 2020, The Astrophysical Journal, 896, 166, doi: 10.3847/1538-4357/ab93cf

Ryan, G., van Eerten, H., Troja, E., et al. 2023, Modelling of Long-Term Afterglow Counterparts to Gravitational Wave Events: The Full View of GRB 170817A, arXiv, doi: 10.48550/arXiv.2310.02328

Sadeh, G. 2024a, Non-thermal emission from mildly relativistic tidal ejecta of compact objects merger, arXiv, doi: 10.48550/arXiv.2406.01338

—. 2024b, Synchrotron break frequencies of mildly-to-highly relativistic outflows observed off-axis. https://arxiv.org/abs/2410.01121v1

Sadeh, G., Guttman, O., & Waxman, E. 2023, Monthly Notices of the Royal Astronomical Society, 518, 2102, doi: 10.1093/mnras/stac3260

Sadeh, G., Linder, N., & Waxman, E. 2024, Monthly Notices of the Royal Astronomical Society, 531, 3279, doi: 10.1093/mnras/stae1286

Synge, J. L. 1957, The Relativistic Gas, North-Holland Publ. Comp., Amsterdam

Takahashi, K., & Ioka, K. 2020, Monthly Notices of the Royal Astronomical Society, 497, 1217, doi: 10.1093/mnras/staa1984

Troja, E., Piro, L., van Eerten, H., et al. 2017, Nature, 551, 71, doi: 10.1038/nature24290

Troja, E., van Eerten, H., Ryan, G., et al. 2019, Monthly Notices of the Royal Astronomical Society, 489, 1919, doi: 10.1093/mnras/stz2248

Troja, E., van Eerten, H., Zhang, B., et al. 2020, Monthly Notices of the Royal Astronomical Society, 498, 5643, doi: 10.1093/mnras/staa2626

Troja, E., O'Connor, B., Ryan, G., et al. 2022, Monthly Notices of the Royal Astronomical Society, 510, 1902, doi: 10.1093/mnras/stab3533

Wang, H., Dastidar, R. G., Giannios, D., & Duffell, P. C. 2024, jetsimpy: A Highly Efficient Hydrodynamic Code for Gamma-ray Burst Afterglow, arXiv, doi: 10.48550/arXiv.2402.19359

Wu, Y., & MacFadyen, A. 2019, The Astrophysical Journal, 880, L23, doi: 10.3847/2041-8213/ab2fd4

Zhang, W., & MacFadyen, A. I. 2006, The Astrophysical Journal Supplement Series, 164, 255, doi: 10.1086/500792

DATA AVAILABILITY

The data underlying this article will be shared following a reasonable request to the corresponding author.

This paper has been typeset from a TeX/LaTeX file prepared by the author.